LAMP/92/2

INTERNATIONAL CENTRE FOR
THEORETICAL PHYSICS

LAMP
SERIES REPORT

(Laser, Atomic and Molecular Physics)

SOLUTIONS OF THE 2-D HELMHOLTZ EQUATION FOR OPTICAL WAVEGUIDES:

Semi-Analytical and Numerical Variational Approaches

A. Sharma

and

P. Bindal

MIRAMARE-TRIESTE

INTERNATIONAL
ATOMIC ENERGY
AGENCY

UNITED NATIONS
EDUCATIONAL,
SCIENTIFIC
AND CULTURAL
ORGANIZATION

International Atomic Energy Agency
and
United Nations Educational Scientific and Cultural Organization
INTERNATIONAL CENTRE FOR THEORETICAL PHYSICS

LAMP SERIES REPORT

(Laser, Atomic and Molecular Physics)

SOLUTIONS OF THE 2–D HELMOHOLTZ EQUATION FOR OPTICAL WAVEGUIDES *

Semi–Analytical and Numerical Variational Approaches

Anurag Sharma **
International Centre for Theoretical Physics, Trieste, Italy

and

Pushpa Bindal
Physics Department, Indian Institute of Technology Delhi,
New Delhi–110016, India.

MIRAMARE – TRIESTE

November 1992

* This is a report based on a LAMP seminar given by A. Sharma while on a visit to ICTP as an Associate.

** Permanent address: Physics Department, Indian Institute of Technology, New Delhi–110016, India.

1 Introduction

Confinement and guidance of electromagnetic waves has been a subject of extensive studies ever since these waves were used as carriers of information. However, with time the frequency of the waves used increased and starting with radio waves, through microwaves, we have now arrived in an era of optical waves. The possibility of using glass fiber waveguides for guidance and transmission of optical waves was suggested by Kao and Hokham in 1966 [1] and a real breakthrough came in 1970 when low loss glass fibers were fabricated at Corning [2]. Since then, over the last two decades, there has been so much development that 'Photonics' is threatening to overshadow electronics in the areas of processing, transmission and storage of information. These and many other developments have been possible with the emergence of integrated optics – a name coined by S.E.Miller in 1969 [3] – in which the optical waves are confined to a small area of space and are processed upon in a variety of ways to achieve operations, such as switching, modulation, coupling, etc., necessary for information processing.

In both optical fibers and integrated optical devices, the basic phenomenon is that of waveguidance, and in order to effectively analyse and design these waveguides, it is neceassary to understand the phenemonon of guidance through them. In the most basic form, this requires the solutions of Maxwell's equations for the boundary conditions represented by the waveguiding structure. Fortunately, for optical waveguides, in most cases of practical importance, the conditions are such that the vector nature of optical waves can be ignored, at least to a very good approximation, and then, it suffices to solve the much simpler Helmholtz equation. This "simpler" Helmholtz equation, however, is still difficult to solve for those integrated optical structures which provide two-dimensional confinement to optical waves (these are the important structures used in the devices). In this case the Helmholtz equation is a partial differential equation and one has to use approximate and/or numerical techniques to obtain its solutions. The present report is concerned with some of such techniques that we have developed recently.

2 Optical Waveguides and the Helmholtz Equation

An optical waveguide is a cylindrical dielectric structure which provides confinement to the waves in the transverse direction while these propagate along the length of the cylinder (usually designated as the z-axis). To provide confinement, it is necessary to have a central region of relatively higher refractive index than that of the the sorrounding region. This central region, where most of the wave energy is confined, is termed as the guiding region (for fibers it is more common to use the term 'core' for this region), whereas the surrounding region is termed as the substrate or the cover (cladding, in case of fibers). The difference in the refractive indices in the two regions is very small (typically less than 1%) and, the waves are nearly (inhomogeneous) plane waves and the scalar approximation can be used, although there are cases where this conditon is not valid. In the present report, however, we will confine our discussion to those cases where it is valid and the scalar approximation holds.

In the case of optical fibers, the cross-section of the cylindrical dielectric structure has circular symmetry and the length of the cylinder is very large, typically, from few meters to several hundreds of kilometers. On the other hand, intergrated optical waveguides

do not have such symmetry in the cross-section (and are, therefore, treated in cartesian coordinates) and the lengths of these waveguides are comparatively very small, typically few hundred micrometers to few millimeters. The waveguides can further be classified as step-index or graded-index depending on whether the refractive-index distribution is piecewise constant or is continuously varying along the transverse direction. It is the latter type of waveguides which are more difficult to analyse. In the present report, we will consider graded index integrated optical waveguides. These are generally referred to as the diffused waveguides or ion-exchange waveguides after the process of fabrication, which involves either diffusion of ions into substrates such as lithium niobate, or exchange of ions in glass substrates.

The refractive index profile of waveguides which provide two-dimensional confinement (these are termed as channel waveguides) can be represented as (see Fig.1a)

$$n^2(x,y) = \begin{cases} n_s^2 + 2n_s\Delta n f(x)g(y) & y > 0 \\ n_c^2 & y < 0 \end{cases} \tag{1}$$

where n_s is the refractive index of the substrate, n_c is the index of the cover (usually air) and Δn is the maximum index change from substrate to the guiding region. In fact, $n_0 = \sqrt{(n_s^2 + 2n_s\Delta n)} \approx n_s + \Delta n$ is the maximum index of the film, generally at the central point ($x = 0$) on the top surface ($y = 0$) of the waveguide film. The Helmholtz equation for such a guiding structure is given by

$$\frac{\partial^2\Psi}{\partial x^2} + \frac{\partial^2\Psi}{\partial y^2} + \frac{\partial^2\Psi}{\partial z^2} + k_0^2 n^2(x,y)\Psi(x,y,z) = 0 \tag{2}$$

where $\Psi(x,y,z)$ is one of the transverse cartesian componets of the electric field. The time dependence of the field is assumed to be of the form $\exp(i\omega t)$ and $k_0 = \omega/c$. Since, the refractive index is independent of z, the z-dependence of Ψ can be separated out and a solution of Eq 2 can be assumed to be of the form

$$\Psi(x,y,z) = \psi(x,y)e^{-i\beta z} \tag{3}$$

where $\psi(x,y)$ satisfies the 2-D Helmholtz equaion

$$\frac{\partial^2\psi}{\partial x^2} + \frac{\partial^2\psi}{\partial y^2} + [k_0^2 n^2(x,y) - \beta^2]\psi(x,y) = 0 \tag{4}$$

and β is a constant referred to as the propagation constant. Equation 4 is in fact an eigenvalue equation with β being the eigenvalue and $\psi(x,y)$ the eigenfunction of the operator $\partial^2/\partial x^2 + \partial^2/\partial y^2 + k_0^2 n^2(x,y)$. Thus, Eq 4 admits only certain discrete solutions, called the guided modes and a continuum of solutions called the radiation modes. It is the guided modes that represent the confinement of waves in the waveguide whereas the radiation modes are not "bound" to the guiding region. The function, $\psi(x,y)$, is the field pattern of the mode and β is the propagation constant of the mode, with ω/β being the phase velocity of the mode inside the waveguide along the z-axis. Depending on the value of Δn and the dimensions of the guiding region, and on the (vacuum) wavelength λ of the propagating wave, a waveguide may support a number of guided modes, each of which, in general, has a different β and $\psi(x,y)$. However, most important waveguides are the ones which allow only one guided mode–the so-called single-mode or monomode

waveguides–since these are the basic elements of most integrated optical devices. Our concern in the present report is also with such waveguides.

If the waveguide is such that it provides only one-dimensional confinement, i.e., if most of the wave energy is confined between two planes, then it is termed as a planar waveguide. Although, these waveguides are rarely used in a device, they are an important stepping stone in the sudy of channel waveguides. The refractive index profile for a planar waveguide can be written as (see Fig.1b)

$$n^2(y) = \begin{cases} n_s^2 + 2n_s\Delta n\ g(y) & y > 0 \\ n_c^2 & y < 0 \end{cases} \tag{5}$$

and the Helmholtz equation reduces a simple differential equation

$$\frac{d^2\phi}{dy^2} + [k_0^2 n^2(y) - \beta^2]\phi(y) = 0 \tag{6}$$

where $\phi(y)$ is the modal field and β is the propagation constant. One can, in general, use a direct numerical method such as the Runge-Kutta method to solve this equation, and use boundary conditions to obtain the propagation constant; however, a number of studies have been devoted to obtain analytical approximations to $\phi(y)$ which provide a better understanding of the guidance in addition to serving as starting point for the analysis of channel waveguides. We shall discuss some of these approximations in Sec 4.

In a channel waveguide, the refractive-index distribution is symmetric along the surface of the waveguide (along the x-direction) and the commonly used functions to model the index variation are

$$f(x) = \begin{cases} \exp(-x^2/W^2) & \text{Gaussian} \\ \left[\text{erf}\left\{\frac{x+W}{D}\right\} - \text{erf}\left\{\frac{x-W}{D}\right\}\right] / [2\text{erf}(W/D)] & \text{error function} \end{cases} \tag{7}$$

On the other hand, the refractive-index distribution along the depth (the y-direction) is highly asymmetric and the commonly used funtional forms for $g(y)$ are

$$g(y) = \begin{cases} \exp(-y/D) & \text{exponential} \\ \exp(-y^2/D^2) & \text{Gaussian} \\ \text{erfc}(y/D) & \text{complementary error function} \end{cases} \tag{8}$$

We have used these representations in our numerical examples.

3 The Variational Principle

The variational principle which has been the basis of a number of methods used in the waveguide theory is based on the integral form of the Helmholtz equation. We have used this principle in developing our analytical models as well as the numerical method discussed in the present report. Therefore, we briefly discuss here the salient features of this principle and its application to waveguide analysis.

The integral form of the Helmholtz equation for a channel waveguide can be written as (see,e.g., [4])

$$\beta^2 = \int\int k_0^2 n^2(x,y)|\psi(x,y)|^2 dxdy - \int\int |\nabla\psi|^2 dxdy \tag{9}$$

where both the integrals are over $-\infty$ to ∞ and it is assumed that the modal field is normalised

$$\int\int |\psi(x,y)|^2 dxdy = 1 \tag{10}$$

The right hand side of Eq 9 is usually referred to as the stationary expression for the propagation constant, β since it is stationary with respect to variations in $\psi(x,y)$. Since the modal field is an unknown function and, in fact, is a function that is sought for as the solution of the propagation problem, one uses an approximation for it as $\psi_t(x,y)$, generally referred to as the trial field. This trial field when used in Eq 9 gives an estimate of the propagation constant, say β_t. Thus, we have

$$\beta_t^2 = \int\int k_0^2 n^2(x,y)|\psi_t(x,y)|^2 dxdy - \int\int |\nabla\psi_t|^2 dxdy \tag{11}$$

Different functions for $\psi_t(x,y)$ would give different values of β_t. An important property of this expression is that all these values of β_t would invariably be smaller than the exact value of β and the exact value is obtained *only* when $\psi_t(x,y)$ is same as the exact modal field [4]. Thus, higher the value of β_t obtained using Eq 11, closer it is to the exact value of β and better is the corresponding $\psi_t(x,y)$ as an approximation for the modal field. Therefore, a value of β_t obtained through the variational expression necessarily represents a better approximation for β than any other approximation which has a smaller value. The same could be concluded about the corresponding approximations for the modal field. This property is extremely useful in developing simple analytical models for the mode of a given waveguide, and the method employed is as follows:

A trial field $\psi_t(x,y;p_1,p_2,\ldots,p_n)$ is set up which involves a number of adjustable parameters $p_1,p_2,\ldots,p_n$. The dependence on x and y is chosen in such a way that ψ_t resembles the actual field as far as possible. This ψ_t is then substituted in the RHS of Eq 11 which is then maximised with respect to the parameters $p_1,p_2,\ldots,p_n$. The maximum value of β_t thus obtained is an estimate for the propagation constant and the corresponding $\psi_t(x,y;p_1,p_2,\ldots,p_n)$ with the optimised valus of parameters $p_1,p_2,\ldots,p_n$ is an approximation for the modal field. Of various $\psi_t(x,y)$ obtained in this manner, the one which gives the largest value of β_t represents the best approximation for the modal field. Generally, by increasing the number of parameters, in a suitable fashion, one can generate better trial fields, but a better trial field with smaller number of parameters is always sought for since it not only simplifies the computations, it is also easier to use for further modelling of devices involving these waveguides.

In case of a planar waveguide, the stationary expression takes the form

$$\beta_t^2 = \int k_0^2 n^2(y)|\phi_t(y)|^2 dy - \int \left|\frac{d\phi_t}{dy}\right|^2 dy \tag{12}$$

where once again the field is assumed to be normalised

$$\int |\phi(y)|^2 dy = 1 \tag{13}$$

Other features of this expression remain the same as discussed above. We use this expression to analyse planar waveguides in the next section.

4 Planar Waveguides

As mentioned above, the Helmholtz equation reduces to an ordinary differential equation for planar waveguides and hence, is much easier to solve. In fact, for a few specific profiles, such as step-index, parabolic-index and sech^2-profile, it is possible to obtain analytical solutions (see, e.g., [5],[6],[7]). However, in the cases of practical importance, particularly asymmetric graded profiles described by Eq 5, analytical solutions are not possible and therefore, a number of numerical and approximate methods have been developed. The approximate methods are generally based on perturbation, WKB and variational techniques. We will, however, confine our discussion to variational methods as these have wider applicability.

4.1 Existing Trial Fields

There are a number of trial fields that have been used in the literature; we, however, focus our attention to two more commonly used ones. Korotky et al.[8] in their study of channel waveguides proposed a trial field using the Hermite-Gauss (HG) functions. This trial field was later used by Mishra and Sharma[9] to study planar waveguides. The trial field for planar waveguides can be written as

$$\phi_{HG}(y) \sim \begin{cases} (y/d)\exp(-y^2/d^2) & y \geq 0 \\ 0 & y \leq 0 \end{cases} \tag{14}$$

where d is the only variational parameter. An important assumption of this trial field is that the field vanishes in the cover region. This is based on the observation that due to large index change at the film-cover interface the field amplitude in very small. Mishra and Sharma[9] also proposed a new trial field based on the cosine and exponential (CE) functions:

$$\phi_{CE}(y) \sim \begin{cases} \cos(p\sigma)\exp[(p\tan p\sigma)(y/d)] & y \leq 0 \\ \cos[p\{(y/d)-\sigma\}] & 0 \leq y \leq \xi d \\ \cos[p(\xi-\sigma)]\exp[-p\tan\{p(\xi-\sigma)\}(y/d-\xi)] & y \geq \xi d \end{cases} \tag{15}$$

where p,σ,ξ are three variational parameters. The CE-field does not assume the field to vanish in the cover region. Table I shows the results for the normalised propagation constant $B = [(\beta/k_0)^2 - n_s^2]/(2n_s\Delta n)$ for various values of the normalised frequency, $V = k_0 D\sqrt{(2n_s\Delta n)}$ for different profile functions defined in Eq 8. While comparing the results obtained using the HG- and CE-fields, it should be recalled that the RHS of Eq 12 has to be maximised with respect to three parameters in the case of the CE-field as against only one parameter in the HG-field. The exact results were obtained using a direct numerical method also described by Mishra and Sharma[9]. Though, CE-results are much better than the HG-results, these still have considerable error inspite of the large number of parameters in the trial field.(The error is typically few percent in B).

4.2 A New Trial Field

In order to investigate further into the nature of these trial fields, we looked at the index profiles for which these trial field are exact modal fields. In other words, using the Helmholtz equation, we found $n^2(y)$ for these $\phi_t(y)$ and β_t. The results are shown in

Fig.2 where the actual index profile- a Gaussian profile- is shown (for $y \geq 0$ region) along with the profiles using the CE- and HG-fields for this Gaussian profile. These results show that the HG-field is totally inadequate in the substrate region and this accounts for its very poor performance for small V-values, since in such cases, the field is less confined to the guiding region and extends deep into the substrate. On the other hand, the CE-field, although approximates well in the substrate region, does not have "enough" graded structure in the guiding region to adequately approximate the profile. This feature remains unchanged at all values of V and is, probably, responsible for the nearly constant error in the values of B. In Fig.2, we have also shown a profile for $g(y) = \text{sech}^2(y/D)$ which fits the given profile remarkably well. This profile, in its symmetric form $[n^2(-y) = n^2(y)]$, allows analytical solutions to the Helmholtz equation. We have used the first antisymmetric mode to construct a new trial field in terms of the secant hyperbolic(SH) function [10]

$$\phi_{SH}(y) \sim \begin{cases} \sinh(y/D)\ \text{sech}^{\tau}(y/D) & y \geq 0 \\ 0 & y \leq 0 \end{cases} \tag{16}$$

where τ is the only parameter. In this trial field also, we have assumed the field to vanish in the cover. The results obtained using this trial field are shown in the last column of Table I. The results are much improved over the HG-results on account of better approximation in the substrate, but are still far less accurate than the CE-results. This is due to the assumption of vanishing field in the cover region. We, therefore, turn our attention to this aspect of the HG- and SH-fields.

4.3 Field in the Cover

We have already mentioned that both HG- and SH-fields are the solutions of the Helmholtz equation for specific profiles–the infinite parabolic and the sech^2, respectively. Both these profiles are in fact symmetric and the HG- and SH-fields are the first antisymmetric modes of these profiles with the field for $y < 0$ suppressed. That the actual modal profile resembles this approximation is apparent from Fig 3 which schematically shows the exact and approximate fields. The main difference between the actual and the approximate fields is the evanescent tail for $y < 0$. Although, one can add another parameter to these approximations and account for the evanescent tail, we have developed [11] a simple method to improve the trial field in the cover region *without* increasing the number of parameters. Our method is based on considering a symmetric index profile which matches the given index profile in the $y \geq 0$ region. Fig 4a shows schematically such a profile. The first antisymmetric mode, $\phi_a(y)$ of this profile matches the SH-(or, HG-)field for $y \geq 0$ (Fig 4c). This profile also has a set of symmetric modes, the first of which, $\phi_s(y)$ is shown in Fig 4b. A suitable sum of these two modes, $\phi_s(y)$ and $\phi_a(y)$, can be constructed in such a way that, in the $y \geq 0$ region, it matches well the mode of the given asymmetric profile (Fig 4d). The field in the $y < 0$ region can then be replaced by an evanescent field which satisfies the Helmholtz equation maintaining the continuity of the field and its derivative at $y = 0$. The improved field obtained in this manner resembles the mode of the given profile remarkably well. The improved field, $\phi_i(y)$ can be written as

$$\phi_i(y) \sim \begin{cases} [\phi_s(y)/\phi_s(0)] + W_c\,[\phi_a(y)/\phi'_a(0)] & y \geq 0 \\ \exp(W_c y) & y \leq 0 \end{cases} \tag{17}$$

where

$$W_c = \sqrt{(\beta_t^2 - k_0^2 n_c^2)} \tag{18}$$

and the value of β_t is obtained using the SH-(or, HG-)field. The improved field, $\phi_i(y)$ contains no variational parameter, and a single evaluation of the RHS of Eq 12 with the improved trial field gives the improved β_t *without* any maximization. In some cases, particularly at very small V-values, the new β_t may be very different from the β_t used in Eq 18. In such cases, the process of improvement should be repeated once with this new β_t in Eq 18.

4.4 Improved Trial Fields

The explicit form of the improved HG- the Evanescent Hermite-Gauss(EHG)- field is then given by

$$\phi_{EHG}(y) \sim \begin{cases} (1 + W_c y)\exp(-y^2/d^2) & y \geq 0 \\ \exp(W_c y) & y \leq 0 \end{cases} \tag{19}$$

with

$$W_c = \sqrt{(\beta_t^2 - k_0^2 n_c^2)} \tag{20}$$

where the values of d and β_t are obtained from the variational expression using the HG-fields as discussed in Sec 4.1.

The expression for the evanescent secant-hyperbolic (ESH) field is given by

$$\phi_{ESH}(y) \sim \begin{cases} [1 + W_c \sinh(y/D)]\text{sech}^{\tau}(y/D) & y \geq 0 \\ \exp(W_c y) & y \leq 0 \end{cases} \tag{21}$$

with

$$W_c = \sqrt{(\beta^2 - k_0^2 n_c^2)} \tag{22}$$

where the values of τ and β_t are obtained using the SH-fields in the variational expression.

Table II shows the results obtained using the EHG and ESH trial fields. The exact results and the CE-results are also included for comparison. The EHG results, though are much improved in comparison to the HG-results, are still in substantial error, particularly for small V-values. This is because the EHG field continues to be inadequate to approximate the field in the substrate. The ESH-results, on the other hand, are very accurate, better than even the results obtained using the CE-field which has three variational parameters (except for very small V-values). The ESH-results are almost coincident with the exact results with typical errors being about 0.1%. This shows that the ESH-field, which still contains only a single parameter, is adequate to approximate the modal field in all the three regions–the cover, the substrate and the guiding region.

5 Channel Waveguides

As already mentioned, channel waveguides provide two-dimensional confinement to the waves and are, in fact, the constituent elements for most of the integrated optical devices. The equation governing propagation in such waveguides, the 2-D Helmholtz equation (Eq 4), being a partial differential, is much more difficult to solve and has therefore been a subject of extensive studies. A variety of numerical methods such as circular harmonic

analysis [12], finite element methods [13],[14], finite difference methods [15],[16],[17], variational methods [18],[19] and the integral equation method [20], and approximate methods such as the Marcatili's method [21], the perturbation method [22], the effective index method [23] and the variational methods [8],[24],[25],[26],[27],[28] have been developed. We will briefly discuss some of the variational methods, and later include the results of some other methods while comparing numerical results.

5.1 The Analytical Trial Fields

The Hermite-Gauss (HG) and the cosine-exponential (CE) trial fields have been developed mainly for channel waveguides; the former for diffused channel waveguids ([8]) and the latter for step-index channel waveguides [25], [26],[27]. The CE-field has later been used for diffused channel waveguides also [28]. A common feature of these methods–in fact, of most approximate methods– is that the trial field $\psi_t(x,y)$ is approximated by a product of a function of x and a function of y, i.e., $\psi_t(x,y)$ is assumed to be separable in x and y:

$$\psi_t(x,y) = \chi(x)\phi(y) \tag{23}$$

Various variational methods differ in their assumptions for the functional forms of $\chi(x)$ and $\phi(y)$. For the HG-field, these are [8]

$$\chi_{HG}(x) \sim \exp(-x^2/\delta^2)$$

$$\phi_{HG}(y) \sim \begin{cases} (y/d)\exp(-y^2/d^2) & y \geq 0 \\ 0 & y \leq 0 \end{cases} \tag{24}$$

where δ and d are the variational parameters. The field in the cover region is again neglected.

The cosine-exponential (CE) field is given by

$$\chi_{CE}(x) \sim \begin{cases} \cos(qx/W) & |x| \leq \eta W \\ \cos(q\eta)\exp[-q\tan(q\eta)(x/W-\eta)] & |x| \geq \eta W \end{cases}$$

$$\phi_{CE}(y) \sim \begin{cases} \cos(p\sigma)\exp[(p\tan p\sigma)(y/d)] & y \leq 0 \\ \cos[p\{(y/d)-\sigma\}] & 0 \leq y \leq \xi d \\ \cos[p(\xi-\sigma)]\exp[-p\tan\{p(\xi-\sigma)\}(y/d-\xi)] & y \geq \xi d \end{cases} \tag{25}$$

where p, q, σ, ξ and η are the five variational parameters.

The secant-hyperbolic (SH) field takes the form

$$\chi_{SH}(x) \sim \mathrm{sech}^{\rho}(x/W)$$

$$\psi_{SH}(y) \sim \begin{cases} \sinh(y/D)\mathrm{sech}^{\tau}(y/D) & y \geq 0 \\ 0 & y \leq 0 \end{cases} \tag{26}$$

where ρ and τ are the variational parameters with field in the cover neglected.

The improvement in HG- and SH-fields on account of the field in the cover can be made exactly in the same manner as described in Sec 4.4. The function $\chi(x)$ remains unchanged in the improved fields. The two variational parameters and β_t are obtained by maximizing the RHS of Eq 11 using the trial field $\chi(x)\phi(y)$. The field $\phi(y)$ is then replaced by the improved trial field obtained using the method described in Sec 4.4. Thus, the EHG-field

is obtained by replacing $\phi_{HG}(y)$ in Eq 24 by $\phi_{EHG}(y)$ of Eq 19, and $\chi_{EHG}(x) = \chi_{HG}(x)$. Similarly, the ESH-field is obtained by replacing $\phi_{SH}(y)$ in Eq 26 by $\phi_{ESH}(y)$ of Eq 21, and $\chi_{ESH}(x) = \chi_{SH}(x)$. Thus, once again, we obtain $\psi_{ESH}(x,y)$ and $\psi_{EHG}(x,y)$ from $\psi_{SH}(x,y)$ and $\psi_{HG}(x,y)$, respectively, *without* addition of any parameter and a *single* evaluation of the RHS of Eq 11 is required in each case for this improvement. An example of numerical values of B obtained using these trial fields is given in Table III. The index profile of the waveguide used is error function along the x-axis (see Eq 7) and Gaussian along the y-axis (see Eq 8) with $W = 3\mu m$ and $D = 3.35\mu m$. There are no exact values available for channel waveguides. In Table III, VOPT refers to a numerical variational method that we have developed and is described in Sec 5.2. As we will discuss in Sec 5.2, this method gives the *best* estimate for β under the assumption of separability (Eq 23). Since the value of B obtained using the VOPT method are largest, these are definitely closer to the exact values (which are still larger than, or equal to, VOPT-values) than the B-values obtained using other trial fields. Thus, the VOPT-values serve as the most accurate values for present comparison. Table III shows that the CE-method, which now has five parameters, is in considerable error, while the EHG or ESH are comparable with the latter being marginally better in accuracy. We shall return to more comparisons in Sec 5.3.

5.2 The Optimal Numerical Variational Method

In the variational methods describe above the accuracy is limited by the assumption of separability (Eq 23) and by the assumption of specific field forms for $\chi(x)$ and $\phi(y)$. We have recently developed a method [29],[30] in which any specific forms for $\chi(x)$ and $\phi(y)$ are not assumed and these are automatically generated by the variational method in the process of optimization. However, the separability is still assumed. Thus, under the assumption of separability, this method generates an *optimal* trial field and gives the *best* accuracy for the propagation constant. The numerical results discussed in Sec 5.3 show this explicitly. We drive the basic equations of the method in Sec 5.2.1 and give the procedure for its implementation in Sec 5.2.2.

5.2.1 Basic Equations

As mentioned above, we continue with the assumption of separability. Thus, with $\psi_t(x,y)$ substituted from Eq 23 into the variational expression, Eq. 11 takes the form

$$\beta_t^2 = \int\int k_0^2 n^2(x,y)|\chi(x)|^2\,|\phi(y)|^2 dxdy - \int |d\chi/dx|^2\,dx - \int |d\phi/dy|^2\,dy \tag{27}$$

where it is assumed that both $\chi(x)$ and $\phi(y)$ are normalised

$$\int |\chi|^2 dx = 1 = \int |\phi|^2 dy \tag{28}$$

Our method is iterative and we assume, to start with, a planar index distribution $n_x^2(x)$ (it could as well be $n_y^2(y)$). We introduce this index distribution into the variational expression of Eq 27 which can be rewritten as [29]

$$\begin{aligned} \beta^2 &= \int k_0^2 n_x^2(x)|\chi(x)|^2 dx - \int |d\chi/dx|^2\,dx \\ &\quad + \int k_0^2|\phi(y)|^2\,[\int\{n^2(x,y) - n_x^2(x)\}|\chi(x)|^2 dx]\,dy - \int |d\phi/dy|^2\,dy \end{aligned} \tag{29}$$

Equations 27 and 29 are identical since the terms containing $n_x^2(x)$ cancel out exactly. However, in writing the equation in this manner, we have separated the RHS in two terms (written on two separate lines). We will show in the following that each of these terms is positive and can be uniquely maximized giving, thus, the maximum value of β_t.

The first term, $\int k_0^2 n_x^2 |\chi|^2 dx - \int |d\chi/dx|^2 dx$ is the variational expression for the planar index profile, $n_x^2(x)$ (*cf.* Eq 12) and hence, is equal to the square of the propagation constant, say β_x^2, of its mode. It is thus, positive and has a maximum value β_x^2. This value can be obtained exactly using a standard numerical method (e.g., the one given in [9]). The function $\chi(x)$ is simply the corresponding modal field which can be normalised to satisfy the condition of Eq 28. We have thus obtained the maximum value of the first term of Eq 29 and have generated the function $\chi(x)$.

The second term of Eq 29 is also in the form of the variational expression for a planar index distribution, $n_y^2(y)$ which is defined as

$$n_y^2(y) = \int \{n^2(x,y) - n_x^2(x)\} |\chi(x)|^2 dx \tag{30}$$

which can be easily evaluated using $n_x^2(x)$ and $\chi(x)$ of the first term. Thus, the second term is also positive and its maximum value is β_y^2, where β_y is the propagation constant of the waveguide defined by $n_y^2(y)$ of Eq 30. The value of β_y and the corresponding modal field $\phi_y(y)$ can be easily obtained numerically. The field $\phi_y(y)$ can then be normalised as required by Eq 28.

Next, we use $n_y^2(y)$ generated above to rewrite the variational expression of Eq 27 as

$$\begin{aligned} \beta^2 &= \int k_0^2 n_y^2(y) |\phi(y)|^2 dy - \int |d\phi/dy|^2 \; dy \\ &\quad + \int k_0^2 |\chi(x)|^2 \left[\int \{n^2(x,y) - n_y^2(y)\} |\phi(y)|^2 dy \right] dx - \int |d\chi/dx|^2 \, dx \end{aligned} \tag{31}$$

The first term on the RHS of Eq 31 is exactly the same as the second term of Eq 29 and has already been maximized. The second term, in Eq 31, is again a variational expression for the index profile $n_x^2(x)$ which is now defined as

$$n_x^2(x) = \int \{n^2(x,y) - n_y^2(y)\} |\phi(y)|^2 dy \tag{32}$$

where $n_y^2(y)$ and $\phi(y)$ are obtained in the first term of Eq 31. The second term, thus, has a maximum value β_x^2 where β_x is the propagation constant of the mode of a waveguide with the profile $n_x^2(x)$ now defined by Eq 32.

This completes one cycle of iteration; starting from an arbitrary $n_x^2(x)$, we have generated a new $n_x^2(x)$ through the variational expression for the given index profile $n^2(x,y)$. This $n_x^2(x)$ is the starting point for the next cycle of iteration. The quantity $\beta_x^2 + \beta_y^2$ gives an estimate of the propagation constant β^2 of the mode of the given channel waveguide $n^2(x,y)$. At the end of each cycle of iteration, one checks for convergence in this quantity and the iterations are stopped when the convergence to a required accuracy is achieved. In most cases, one requires 2–3 iteration to obtain convergence to about 4 digits in B.

5.2.2 Implementation Procedure

The method described in Sec 5.2.1 can be implemented as an iterative procedure for obtaining the propagation characteristics of a channel waveguide. Various steps required for this implementation are outlined below:

STEP 1: Choose an $n_x^2(x)$. A good choice is $n_x^2(x) = n^2(x, y = 0)$.
STEP 2: Obtain β_x^2 and $\chi(x)$ numerically. Normalize $\chi(x)$.
STEP 3: Obtain $n_y^2(y)$ using Eq 30.
STEP 4: Obtain β_y^2 and $\phi(y)$ numerically for $n_y^2(y)$. Normalize $\phi(y)$.
STEP 5: Obtain $n_x^2(x)$ using Eq 32.
STEP 6: Obtain β_x^2 and $\chi(x)$ numerically for $n_x^2(x)$. Normalize $\chi(x)$.
STEP 7: Compute $\beta_t^2 = \beta_x^2 + \beta_y^2$. Check for convergence in β_t^2.
IF Converged, GOTO STEP 8
OTHERWISE, GOTO STEP 3
STEP 8: β_t^2 and $\psi_t(x,y) = \chi(x)\phi(y)$ are the required propagation constant and modal field.

For translation of this procedure into a computer program, one requires the following three elements:

1. Computation of the propagation constant of a planar waveguide. We have used the Ricatti transformation [9] and have solved the resulting first order differential equation using the predictor-corrector method [31].
2. Computation of the modal field. We have used the predictor-corrector method for the Helmholtz equation directly.
3. Integration over the field to normalise it and to obtain the index distribution in the orthogonal direction (Eq 30 or Eq 32). We have used Bode's 4-point formula [31] for evaluation of integrals, since the truncation error of this formula is of the same order as that of the predictor- corrector method.

Other details for implementation are given in Sharma and Bindal[30].

5.3 Numerical Results and Comparisons

We discuss in this section some specific numerical examples to show the accuracies of various methods discussed above in comparison to other available methods. In particular, we will include the following methods in our comparisons:

1. VFD: Scalar finite difference method based on the variational principle. Numerical results have been obtained using a 14x14 mesh point grid in the transverse cross-section ([16])
2. HFD: A direct vector finite-difference method based on the magnetic (H) field components with typically 20x20 mesh point grid in the transverse cross-section ([17])
3. HG: The Hermite-Gauss method of Korotky et al. [8] discussed in Sec 5.1
4. EHG: Variational method with Evanescent Hermite-Gauss trial field ([11]) discussed in Sec 5.1.
5. SH & ESH: Variational method with secant hyperbolic (SH) and evanescent secant hyperbolic (ESH) trial fields [10] discussed in Sec 5.1
6. VOPT: The optimal variational method discussed in Sec 5.2. Typically 200 points are used for each one-dimensional analysis, and 3 or less iterations are required for each V-value ([30])

The first numerical example is for an error function-Gaussian profile (error function in the x-direction and Gaussian in the y-direction). This profile has been studied by Korotky et al.[8]. Fig 5a shows the results obtained the HG, EHG and VOPT methods while Fig 5b shows the results for the SH, ESH and VOPT methods. These results show that both EHG and ESH are close to VOPT results with ESH-results being nearly coincident with VOPT-results for the range of V-values which are important for single mode operation. This shows that the ESH-field is an extremely good approximation for mode of such a waveguide. The next example is a Gaussian-exponential profile which has been studied by Schulz et al. [17] using the HFD-method. The results are given in Fig 6 where the ESH-results are also included. This figure shows that the HFD-results are grossly inaccurate while the ESH-results are once again extremely close to the VOPT-results which are definitely closest to the exact results as these represent the largest values of β. Another comparison with finite-difference methods is shown in Fig 7, in which results for a Gaussian-Gaussian profile are given. The figure includes results obtained using the VOPT, ESH, HFD and VFD methods. This figure also shows that the finite-difference methods (both HFD and VFD) give very poor accuracy whereas ESH continues to be extremely accurate and almost coincident with VOPT-results except for very small V-values. The low accuracy of the VFD- and HFD-results can be ascribed to rather small size, 14x14 and 20x20, respectively, of the grid for sampling the field in the transverse cross-section. In the case of VOPT, in which one has to consider only a one-dimensional sampling of the field at a time, the field is sampled, in effect, on a grid of size 200x200. In addition, in the finite difference methods, one assumes that the field vanishes at the boundaries of a window whose size is kept large enough in order to keep the effect of this approximation at a negligible level. However, larger the size of the window, more are the grid points required to sample the field so that these are close enough to approximate its variation adequately. On the other hand, in VOPT, the field is assumed to decay exponentially out side the computationl grid. These two aspects of finite-difference (and also finite-element) methods limit the accuracy rather severely unless very large computer memory and time are at disposal. The grid sizes of 20x20, used in HFD, and 14x14, used in VFD, are highly inadequate as shown by above results. More examples are given in Refs. [10] and [30] which further confirm the conclusions drawn here.

6 Equivalent 1-D Profiles for Channel Waveguides

In the numerical method discussed in Sec 5.2, two 1-D index profiles $n_x^2(x)$ and $n_y^2(y)$ are generated for the given 2-D profile $n^2(x,y)$. These 1-D profiles can be used to obtain "equivalent" 1-D profiles for the given 2-D profile. Thus, we can define ([29],[32])

$$n_{x_{eq}}^2(x) = \int \{n^2(x,y) - n_y^2(y)\}|\phi(y)|^2 dy + \beta_t^2/k_0^2 \tag{33}$$

and

$$n_{y_{eq}}^2(y) = \int \{n^2(x,y) - n_x^2(x)\}|\chi(x)|^2 dx + \beta_t^2/k_0^2 \tag{34}$$

where $n_x^2(x)$, $n_y^2(y)$, $\chi(x)$, $\phi(y)$ and β_t are obtained at the state of convergence in the numerical method of Sec 5.2 for the given index profile $n^2(x,y)$.

The index profiles $n^2(x,y)$ and, say, $n_x^2(x)$ are equivalent in the following sense. The modes for both the profiles have the same propagation constant, β_t, and have identical

x-variation of the modal fields. In other words, the propagating modal field $\chi(x)e^{-i\beta_t z}$ of the equivalent profile $n_{x_{eq}}^2(x)$ is a projection on the x-z plane of the propagating modal field $\psi_t(x,y)e^{-i\beta_t z}$ of the given waveguide $n^2(x,y)$. This equivalent profile can be used to simulate or model interactions between different waveguides in the x-z plane. These simulations can be expected to be reasonably accurate in a number of practical cases. We discuss, in the next section, a specific example of an integrated optical component–the directional coupler, and show expliciltly the accuracy of equivalent waveguides.

7 Directional Couplers

Directional couplers are the basis for a variety of integrated optical devices such as switches, modulators, and power dividers. A directional coupler consists of two identical waveguides placed parallel to each other along the z-axis separated by a constant distance (see Fig 8).(In some special applications, the waveguides may be non-identical and/or the separation between them may not be constant). The modes of the two waveguides, due to the overlap of their evanescent fields, get coupled to each other and exchange power between them as they propagate along the z-axis.

Diffused waveguide directional couplers have been widely studied, both experimentally [33],[34],[35] and theoretically [24],[34],[36],[37], [38], [39],[40]. Most earlier studies either neglected the variation of refractive index in the direction normal to the directional coupler [34] or used the effective index method [23] to reduce the 2-D profile to a 1-D profile ([33],[36],[38],[39]). The first analysis taking full 2-D index profile into account was carried out by Jain et al.[24]. Later, Hawkins and Goll [40] presented a variational analysis modifying the Hermite-Gauss (HG) trial field ([8] and Sec 5.1). Another approach was developed by Fiet and Fleck [37] which was computationally intensive. We briefly discuss the basic characteristics of a directional coupler in Sec 7.1 and then, use the numerical method of Sec 5.2 along with the concept of equivalent waveguides (Sec 6) to obtain the important characteristics from the index distribution. In Sec 7.2, we discuss an evanescent secant-hyperbolic (ESH) model for these couplers and finally, present some results including comparisons with other theoretical and experimental results in Sec 7.3.

7.1 Basic Characteristics of Directional Couplers

The refractive index profile for a directional coupler made up of two diffused channel waveguides can be written as (Fig 8)

$$n^2(x,y) = \begin{cases} n_s^2 + 2n_s\Delta n g(y)[f(x-s) + f(x+s)] & y > 0 \\ n_c^2 & y < 0 \end{cases} \tag{35}$$

where $2s$ is the separation between the centres of the two constituent channel waveguides. The composite waveguiding structure thus formed has two modes one of which is symmetric and the other is antisymmetric. The propagation constant of these modes, β_s and β_a, respectively, depend on the separation parameter, s, and are such that $\beta_s \geq \beta \geq \beta_a$ (β being the propagation constant of the isolated waveguide). The equality holds when the waveguides are widely separated (lage values of s), so that their evanescent fields (along x) have become vanishingly small and there is no interaction between them. In this limit, $\beta_s, \beta_a \to \beta$. Due to different propagation constants, the modes propagate with different

phase velocities and hence, acquire phase at different rates as they propagate along the length of the directional coupler, the z-axis. This leads to a z-dependent phase difference between them which shows up as intensity variation along the z-axis (since they have different field distributions). The effect of this characteristics is that when light is launched in one the waveguides, say the one centered at $x = -s$, the two modes of the directional coupler are simultaneously excited, say in phase. After propagating through a certain distance, the modes will be exactly out of phase and the intensity will be maximum in the other waveguide (centered at $x = s$). Thus, in effect, the power has transferred from one waveguide to another waveguide. This distance, after which maximum power is transferred from one waveguide to the other, is called the coupling length, l_c and is defined as

$$l_c = \frac{\pi}{\beta_s - \beta_a} \tag{36}$$

This coupling length is the main parameter of a directional coupler and diffenrent methods have been used to obtain its value from the given refractive index profile. We discuss some of these methods in the next section.

7.2 2-D and Equivalent 1-D Numerical Methods

As mentioned above, in order to obtain the coupling length, l_c, of a directional coupler, one has to obtain the propagation constants of the first symmetric and the first antisymmetric modes, β_s and β_a, respectively. In the 2-D numerical method, the composite waveguiding structure, defined by Eq 35 is considered to be one waveguide and its first two modes are obtained, indivisually, using the numerical method VOPT (described in Sec 5.2). The coupling length of the coupler (Eq 36) is then computed using the propagation constants of these modes.

In the equivalent 1-D approach, one first uses the VOPT method for a single constituent waveguide of the directional coupler and obtains the equivalent 1-D profile, $n^2_{x_{eq}}(x)$ as described in Sec 6. The equivalent profile $n^2_{x_{eq}}(x)$ is then used to construct an equivalent 1-D directional coupler with index profile given by

$$n^2_{eq}(x) = n^2_{x_{eq}}(x - s) + n^2_{x_{eq}}(x + s) - n^2_{s_{eq}} \tag{37}$$

where $n^2_{s_{eq}}$ is the constant substrate index of $n^2_{x_{eq}}(x)$ (this is the value of $n^2_{x_{eq}}(x)$ for very large x). Using any standard numerical method one can obtain the propagation constants of the first two modes of the planar index distribution, $n^2_{eq}(x)$, defined in Eq 37. These propagation constants approximate very well the propagation constants of the symmetric and the antisymmetric modes of the given dirctional coupler and hence, give directly the coupling length, l_c through Eq 36.

To show the accuracy of the equivalent 1-D approach, we have carried out [32] computations for directional couplers fabricated by Noda et al.[34]. The values of coupling lengths obtained by the 2-D numerical method and the equivalent 1-D method are given in Table IV. These results show that the equivalent 1-D directional coupler is nearly as good as the real 2-D directional coupler. The equivalent 1-D directional coupler, however, requires much less computational effort. In particular, if the coupling length is desired for several values of waveguide separation parameter, s, then in the 2-D case, one will have to repeat the VOPT method for each values of s. On the other hand, in the equivalent 1-D method, the VOPT method is required only once to obtain the $n^2_{x_{eq}}(x)$ and for each

value of s one has to analyse only the 1-D directional coupler (Eq 37) to obtain modes and the coupling length.

7.3 The ESH-Field Analysis for Directional Couplers

In Sec 5.1, we have discussed the evanescent secant-hyperbolic (ESH) trial field for the analysis of channel waveguides. We now extend the same model to obtain the coupling length of directional couplers made of two such waveguides. The concept of equivalent waveguides is implicitly used in this model. Various steps of analysis are summarised below:

- Use the secant-hyperbolic (SH) trial field for a single contituent waveguide to obtain ρ and τ:

$$\chi_{SH}(x) \sim \mathrm{sech}^{\rho}(x/W)$$

$$\phi_{SH}(y) \sim \begin{cases} \sinh(y/D)\mathrm{sech}^{\tau}(y/D) & y \geq 0 \\ 0 & y \leq 0 \end{cases}$$

- Modify $\phi(y)$ to include the field in the cover (i.e., derive an ESH field)

$$\chi_{ESH}(x) \sim \mathrm{sech}^{\rho}(x/W)$$

$$\phi_{ESH}(y) \sim \begin{cases} [1 + W_c \sinh(y/D)]\mathrm{sech}^{\tau}(y/D) & y \geq 0 \\ \exp(W_c y) & y \leq 0 \end{cases}$$

- Use $\chi_{ESH}(x)$ to construct the symmetric and the antisymmetric fields:

$$\chi_s(x) \sim \mathrm{sech}^{\rho}[(x - s)/W] + \mathrm{sech}^{\rho}[(x + s)/W] \tag{38}$$

$$\chi_a(x) \sim \mathrm{sech}^{\rho}[(x - s)/W] - \mathrm{sech}^{\rho}[(x + s)/W] \tag{39}$$

- Using $\chi_s(x)\phi_{ESH}(y)$ and $\chi_a(x)\phi_{ESH}(y)$ in the variational expression (Eq 11), one obtains β_s and β_a, respectively, *without* any maximization.
- Obtain coupling length, l_c, using these β_s and β_a in Eq 36.

In this way, coupling length can be obtained without any maximization. This analysis is fairly accurate for relatively large values of s. However, for small values of s, when the waveguide modes influence each other rather strongly, a modification is necessary. In such cases, the peaks of the modes are no longer at the points where the index has the largest value. In fact, the peaks of the symmetric modes come closer to each other while those of antisymmetric modes becomes farther apart. This possiblity is not taken into consideration in Eqs 38 & 39. To take this aspect into account, we can modify the modes for the symmetric and the antisymmetric mode by introducing a parameter, σ such that

$$\chi_s(x;\sigma) \sim \mathrm{sech}^{\rho}[(x - \sigma)/W] + \mathrm{sech}^{\rho}[(x + \sigma)/W] \tag{40}$$

$$\chi_a(x;\sigma) \sim \mathrm{sech}^{\rho}[(x - \sigma)/W] - \mathrm{sech}^{\rho}[(x + \sigma)/W] \tag{41}$$

The values of σ are such that $\sigma \leq s$ for the symmetric mode and $\sigma \geq s$ for the antisymmetric mode, and $\sigma \to s$ for both modes for $s \gg W$. The parameter σ is treated as a variational parameter for maximizing the variational expression (Eq 11) for the trial fields $\chi_s(x;\sigma)\phi_{ESH}(y)$ and $\chi_a(x;\sigma)\phi_{ESH}(y)$ to obtain β_s and β_a. These values of propagation constant then give improved value of the coupling length, l_c.

7.4 Numerical Results and Comparisons

We present in this section few examples to show the accuracy of the methods that we have discussed in Secs 7.2 and 7.3 for directional couplers. In the first example we again consider the directional couplers fabricated by Noda et al.[34]. The profile assumed is Gaussian-Gaussian (see Eqs 7 & 8) with parameters $n_s = 2.152$, $n_c = 1.0$, $\lambda = 1.153\mu$m, $W = 4.0\mu$m and $D = 5.0\mu$m. The results are shown in Fig 9. Two cases with $\Delta n = 0.004$ and $\Delta n = 0.006$ are included. Experimental results of Noda et al.[34] and the theoretical results using VOPT and ESH are included in the figure. Another example is shown in Fig 10 where we have considered the directional couplers reported by Korotky and Alferness [35]. The profile assumed is error function-Gaussian with parameters $n_s = 2.1398$, $n_c = 1.0$, $\lambda = 1.32\mu$m, $W = 4.0\mu$m and $D = 3.8\mu$m. The metal strip thickness is 0.068μm which controls the value of Δn ([8],[35]). Figure 9 also shows the theoretical results of Hawkins and Goll [40] along with the results obtained using VOPT and ESH. These figures show that the results obtained using VOPT and ESH methods are in very good agreement with the experimental data. This again brings out the point that VOPT and ESH methods are extremely good methods for modeling and analysis of channel waveguides and devices made with these waveguides.

8 Summary

We have presented in this report some of the recent work on the analysis of diffused waveguides and directional couplers. We have developed [11] a simple way to improve the Hermite-Gauss (HG) trial field [8] for the field in the cover region. We have also presented [10] a better trial field–the secant-hyperbolic field, which is much more accurate than the HG-field while it retains the simplicity of the HG-field. The improved version of this field–the evanescent secant-hyperbolic field [10], is extremely accurate and compares well with the numerical methods which require much more computational effort.

We have also developed [30] a numerical method (VOPT) which gives the best accuracy in the propagation constant under the assumption that the trial field can be separated in its functional dependence on the width and the depth coordinates. This assuption, our results show, holds good for diffused channel waveguides. The numerical results show that, at least for the cases that we have discussed, the finite difference (FD) methods give extremely poor accuracies in comparison to our method. In fact, even simple approximations such as the HG- and SH-trial fields are better than these FD methods. This could be due to rather small number of field sample points taken in these methods. The computational effort in an FD method is orders of magnitude more than the methods that we have described.

We have also included analysis of diffused channel waveguide directional couplers mainly to illustrate an application of the methods we have developed. Comparisons with experimental data again show that the ESH method and the numerical method (VOPT) perform extremely well in predicting the coupling length of directional couplers.

9 Acknowledgements

One of the authors (A.S.) would like to thank Professor Abdus Salam, the International Atomic Energy Agency and the UNESCO for the hospitality at the International Centre for Theoretical Physics, Trieste. He has also been a Homi Bhabha Fellow during the course of the work reported here. The work has mostly been carried out at I.I.T. Delhi with partial support from the Council of Scientific and Industrial Research (India).

References

[1] C.Kao and G.A.Hokham, "Dielectric-Fiber Surface Waveguide for Optical Frequencies", Proc. IEE **133**, 1151 (1966).

[2] F.P.Kapron, B.D.Keck and R.D.Maurer, "Radiation Losses in Glass Optical Waveguides", Appl. Phys. Lett. **17**, 423 (1970).

[3] S.E.Miller, "Integrated Optics: An Introduction", Bell Syst. Tech. J. **48**, 2059 (1969).

[4] H.Kogelnik, "Theory of optical waveguides" in *Integrated Optics*, T.Tamir (Ed.), Springer Verlag, Berlin, 1975, p.44.

[5] A.K.Ghatak and K.Thyagarajan, *Optical Electronics*, Cambridge University Press, Cambridge, 1989.

[6] A.W.Snyder and J.D.Love, *Optical Waveguide Theory*, Chapman & Hall, London, 1983.

[7] M.J.Adams, *An Introduction to Optical Waveguides*, Wiley, Chichester, 1981.

[8] S.K.Korotky, W.J.Minford, L.L.Buhl, M.D.Divino, and R.C.Alferness," Mode size and method for estimating the propagation constant of single mode Ti:$LiNbO_3$ strip waveguides", IEEE J. Quant. Electron. **QE-18**, 1796 (1982).

[9] P.K.Mishra and A.Sharma," Analysis of Single Mode Inhomogenous Planar Waveguides", J. Lightwave Technol. **LT-4**, 204 (1986).

[10] A.Sharma and P.Bindal, "Variational Analysis of Diffused Planar and Channel Waveguides and Directional Couplers", submitted to J. Opt. Soc. Am. A.

[11] A.Sharma and P.Bindal, "Analysis of Diffused Planar and Channel Waveguide", IEEE J. Quant. Electron. (in press).

[12] J.E.Goell,"A Circular-Harmonic Computer Analysis of Rectangular Dielectric Waveguides", Bell Syst. Tech. J. **48**, 2133 (1969).

[13] B.M.A.Rahman and J.B.Davies, "Finite-Element Solution of Integrated Optical Waveguides", J. Lightwave Technol. **LT-2**, 682 (1984).

[14] C.Yeh, K.Ha, S.B.Dong and W.P.Brown, "Single-Mode Optical Waveguides", Appl.Opt. **18**, 1490 (1979).

[15] K.Bierworth, N.Schulz and F.Arndt,"Finite Difference Analysis of Rectangular Dielectric Waveguide Structures", IEEE Trans. Microwave Theory Tech. **MTT-34**, 1104 (1986).

[16] R.K.Lagu and R.V.Ramaswamy " A Variational Finite Difference Method for Analysing Channel Waveguides with Arbitrary Index Profiles," IEEE J. Quant. Electron. **QE-22**, 968 (1986).

[17] N.Schulz, K.Bierwirth, F.Arndt, and U.Koster ," Finite Difference Method without Spurious Solutions for the Hybrid-Mode Analysis of Diffused Channel Waveguides," IEEE Trans. Microwave Theory Tech. **MTT-38**, 722 (1990).

[18] M.Matsuhara, "Analysis of TEM Modes in Dielectric Waveguides by a Variational Method", J. Opt. Soc. Am. **63**, 1514 (1973).

[19] H.F.Taylor, "Dispersion Characteristics of Diffused Channel Waveguides", IEEE J. Quant. Electron. **QE-12**, 748 (1976).

[20] Ch.Pichot, " Exact Numerical Solution for the Diffused Channel Waveguide", Optics Commun. **41**, 169 (1982).

[21] E.A.J.Marcatili, "Dielectric Rectangular Waveguide and Directional Coupler for Integrted Optics", Bell Syst. Tech. J. **48**, 2071 (1969).

[22] A.Kumar, K.Thyagarajan and A.K.Ghatak, "Analysis of Rectangular-Core Dielectric Waveguides: An Accurate Perturbation Approach", Opt. Lett. **8**, 63 (1983).

[23] G.B.Hocker and W.K.Burns, "Mode Dispersion in Diffused Channel Waveguides by the Effective Index Method", Appl. Opt. **16**, 113 (1977).

[24] U.Jain, A.Sharma, K.Thyagarajan and A.K.Ghatak," Coupling Characteristics of a Diffused Channel Waveguide Directional Coupler," J. Opt. Soc. Am. **72** , 1545 (1982).

[25] A.Sharma, P.K.Mishra and A.K.Ghatak," Analysis of Single Mode Waveguides and Directional Couplers with Rectangular Cross Section," Proceedings of 2nd European Conference on Integrated Optics (Florence,Italy), October 17–18, (1983), pp.9–12.

[26] P.K.Mishra, A.Sharma, S.Labroo and A.K.Ghatak, "Scalar Variational Analysis of Single-Mode Waveguides with Rectangular Cross-section", IEEE Trans. Microwave Theory Tech. **MTT-33**, 282 (1985).

[27] A.Sharma, P.K.Mishra and A.K.Ghatak, "Single-Mode Optical Waveguides and Directional Couplers with Rectangular Cross Section: A Simple and Accurate Method of Analysis", J. Lightwave Technol. **6**, 1119 (1988).

[28] P.K.Mishra and A.Sharma, "Analysis of Diffused Channel Waveguides", in 18th Optical Society of India Symposium, Bangalore (India), March 21-23, 1990.

[29] A.Sharma, "On Approximate Theories of Single Mode Rectangular Waveguides", Opt. Quantum Electron. **21**, 517 (1989).

[30] A.Sharma and P.Bindal," An Accurate Variational Analysis of Single Mode Diffused Channel Waveguides," Opt. Quantum Electron. (in press).

[31] M.Abramowitz and I.A.Stegun, *Handbook of Mathematical Functions*, Dover, New York, 1970.

[32] P.Bindal and A.Sharma," Modelling of Ti:$LiNbO_3$ Directional Couplers," IEEE Photon. Technol. Lett. (in press).

[33] R.C.Alferness, R.V.Schmidt, and E.H.Turner, "Characteristics of Ti-Diffused Lithium Niobate Optical Directional Couplers," Appl. Opt. **18**, 4012 (1979)

[34] J.Noda, M.Fukuma and O.Mikami," Design Calculations for Directional Couplers Fabricated by Ti-diffused $LiNbO_3$ Waveguides," Appl.Opt. **20**, 2284 (1981).

[35] S.K.Korotky and R.C.Alferness, "The Ti:$LiNbO_3$ Integerated-Optic Technology: Fundamentals, Design Considerations and Capabilities," in *Integerated Optical Circuits and Components*, L.D.Hutcheson (Ed.), Marcel Dekker, New York, 1987.

[36] A.Sharma, E.Sharma, I.C.Goyal and A.K.Ghatak, "Variational Analysis of Directional Couplers with Graded-Index Profile", Opt. Commun. **34**, 39 (1980).

[37] M.D.Fiet and J.A.Fleck, Jr., "Comparison of Calculated and Measured Performance of Diffused Channel-Waveguide Couplers," J. Opt. Soc. Am. **73**, 1296 (1983).

[38] J.Ctyroky, M.Hofman, J.Janta, and J.Schrofel," 3-D Analysis of $LiNbO_3$:Ti Channel Waveguides and Directional Couplers," IEEE J. Quant. Electron. **QE-20**, 400 (1984).

[39] C.M.Kim and R.V.Ramaswamy, "WKB Analysis of Asymmetric Directional Couplers and its Application to Optical Switches," J. Lightwave Technol. **6**, 1109-1118 (1988).

[40] R.T.Hawkins and J.H.Goll," Method for Calculating Coupling Length of Ti:$LiNbO_3$ Waveguide Directional Couplers," IEEE J. Ligtwave Technol. **6**, 887 (1988).

Table I Results for Planar Waveguides: Values of $B = [(\beta/k_0)^2 - n_s^2]/2n_s\Delta n$

$g(y)$	V	Exact	CE	HG	SH
$\exp(-y^2/D^2)$	2.0	0.082	0.078	0.005	0.036
	3.0	0.275	0.270	0.216	0.227
	4.0	0.413	0.408	0.370	0.374
$\exp(-y/D)$	2.0	0.105	0.100	0.066	0.077
	3.0	0.229	0.223	0.193	0.201
	4.0	0.321	0.316	0.289	0.295
$\mathrm{erfc}(y/D)$	3.0	0.068	0.064	0.015	0.043
	4.0	0.169	0.164	0.121	0.131

Table II Results for Planar Waveguides: Values of $B = [(\beta/k_0)^2 - n_s^2]/2n_s\Delta n$

$g(y)$	V	Exact	EHG	ESH	CE
$\exp(-y^2/D^2)$	2.0	0.082	0.044	0.076	0.078
	3.0	0.275	0.263	0.274	0.270
	4.0	0.413	0.408	0.413	0.408
$\exp(-y/D)$	2.0	0.105	0.087	0.102	0.100
	3.0	0.229	0.218	0.228	0.223
	4.0	0.321	0.313	0.319	0.316
$\mathrm{erfc}(y/D)$	3.0	0.068	0.041	0.067	0.064
	4.0	0.169	0.154	0.164	0.164

Table III Results for Channel Waveguides: Values of $B = [(\beta/k_0)^2 - n_s^2]/2n_s\Delta n$

V	V_{OPT}	HG	EHG	SH	ESH	CE
2.12	0.133	0.112	0.125	0.118	0.130	0.123
2.59	0.248	0.233	0.247	0.231	0.245	0.234
3.00	0.329	0.313	0.328	0.313	0.327	0.318

Table IV Results for Directional Couplers: Values of Coupling Length, l_c in mm

Process Parameters	2-D Analysis	1-D Analysis
Δn=0.006 s=6.08 μm	5.7965	5.8016
Δn=0.006 s=6.56 μm	10.5211	10.5360
Δn=0.004 s=6.08 μm	3.6956	3.6892
Δn=0.004 s=6.56 μm	5.5469	5.5463

Figure Captions

Fig 1: Schematic of the refractive index distribution in (a) a diffused channel waveguide and (b) a diffused planar waveguide.

Fig 2: Refractive index profiles corresponding to various trial fields for a diffused planar waveguide with a Gaussian index profile.

Fig 3: Schematic of (a) the index profile of a diffused planar waveguide, (b) field distribution of its mode, and (c) the HG or SH trial field.

Fig 4: Schematic of (a) a symmetric profile corresponding to a given diffused planar waveguide, (b) its symmetric mode, (c) its antisymmetric mode, (d) a sum of these two modes, and (e) the sum with an evanescent field for $y < 0$.

Fig 5: (a & b) Normalised propagation constant, B as a function of the normalised frequency, V for a diffused channel waveguide with an error function-Gaussian profile with parameters: $n_s = 2.203$, $n_c = 1.0$, $\lambda = 1.3\mu$m, $D = 3.35\mu$m and $W = 3.0\mu$m.

Fig 6: Normalised propagation constant, B as a function of V for a diffused channel waveguide with Gaussian-exponential profile with parameters: $n_s^2 = 2.0$, $n_c = 1.0$, $\lambda = 1.3\mu$m, $D/W = 1$ and $n_0 = 1.05n_s$.

Fig 7: Normalised propagation constant, B as a function of V for a diffused channel waveguide with Gaussian-Gaussian profile with parameters: $n_s^2 = 2.1$, $n_c = 1.0$, $\lambda = 1.3\mu$m, $D/W = 1$ and $n_0 = 1.05n_s$.

Fig 8: Schematic of the index profile of a directional coupler made of two parallel diffused channel waveguides.

Fig 9: Coupling length, l_c as a function of s, one half of the waveguide separation for a directional coupler reported by Noda et al.[34].

Fig 10: Coupling length, l_c as a function of s, one half of the waveguide separation for a directional coupler reported by Korotky and Alferness[35]. Theoretical results obtained by Hawkins and Goll[40] are also shown.

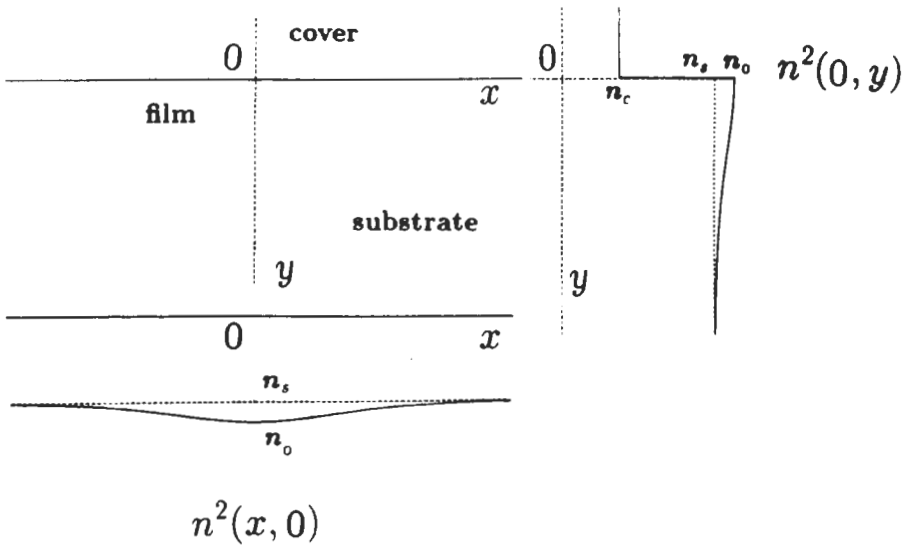

(a)

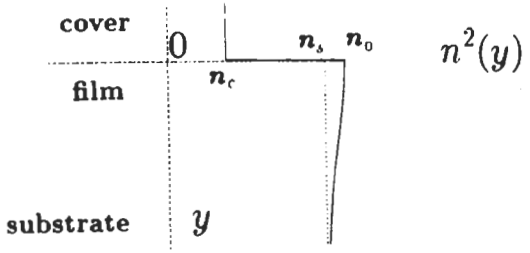

(b)

Fig 1

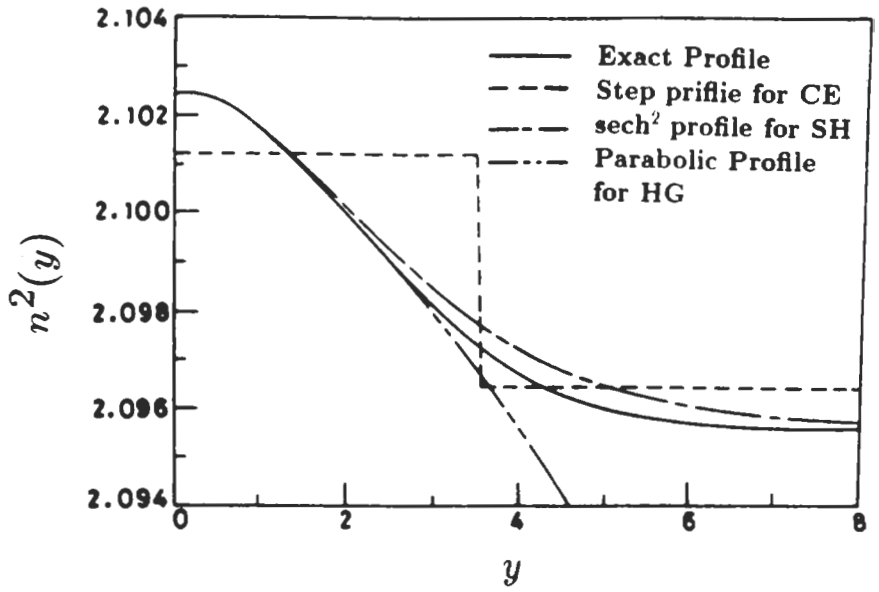

Fig 2

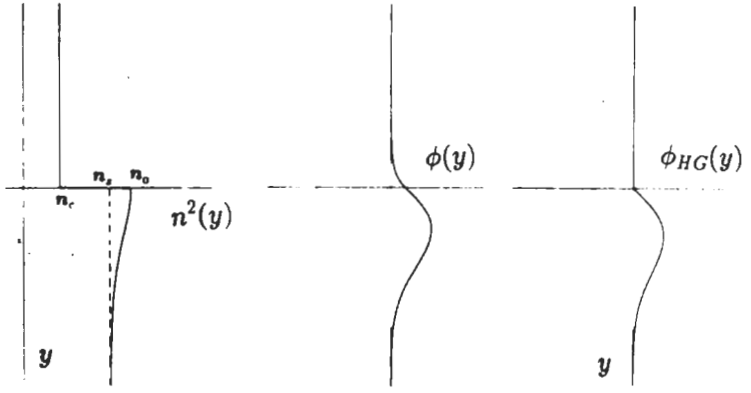

(a) (b) (c)

Fig 3

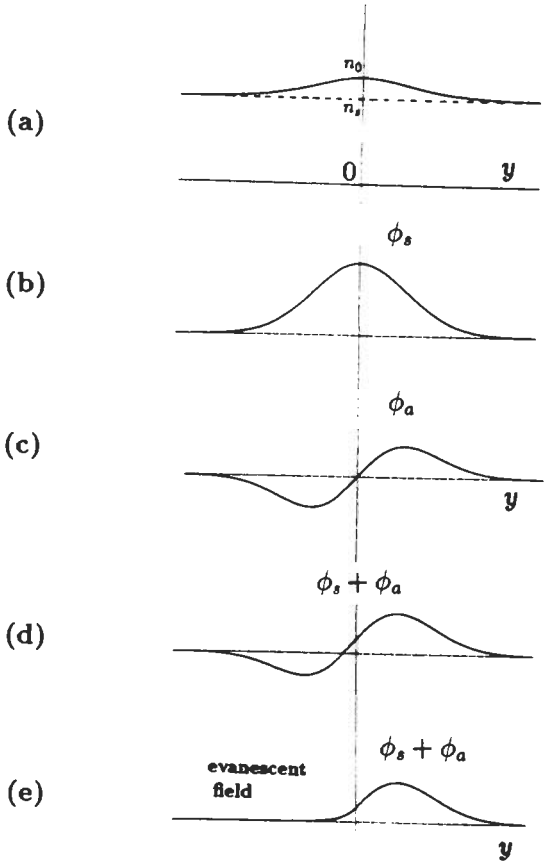
(a)
n_0
n_s
0
y
(b)
ϕ_s
(c)
ϕ_a
y
(d)
$\phi_s + \phi_a$
(e)
evanescent field
$\phi_s + \phi_a$
y

Fig 4

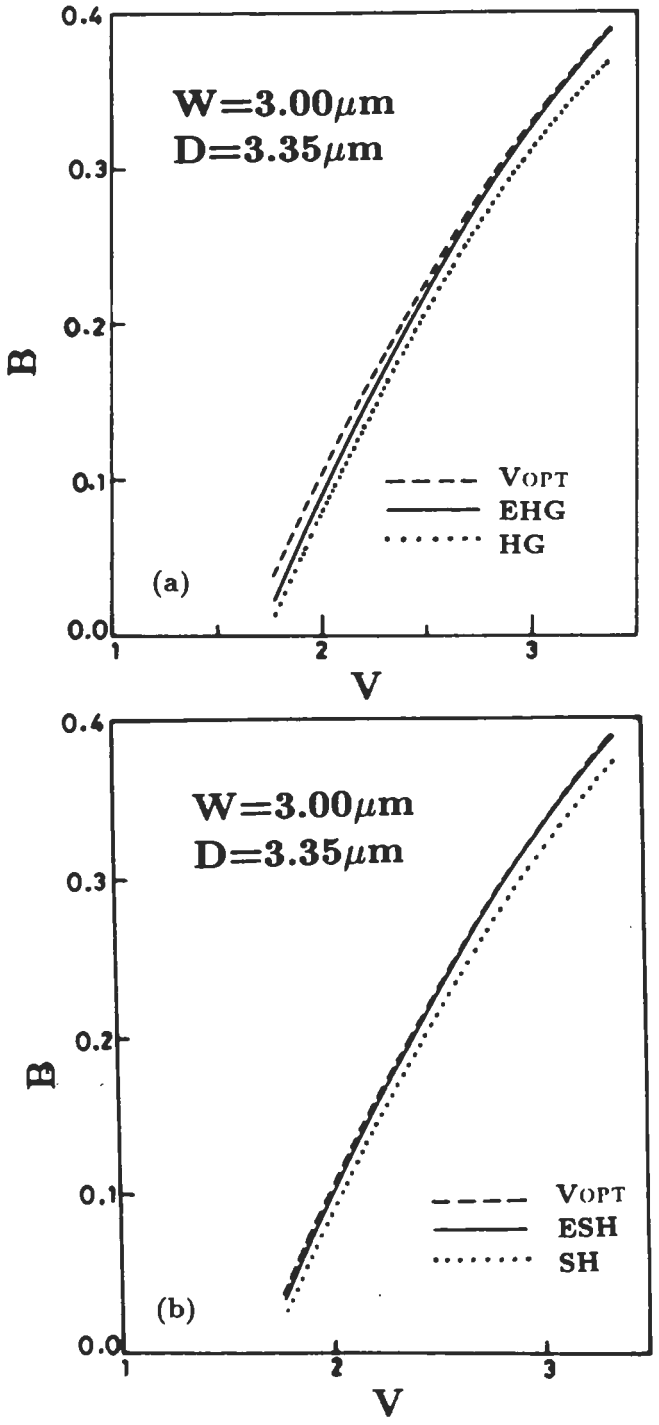
W=3.00μm
D=3.35μm
VOPT
EHG
HG
(a)
B
V
0.0
0.1
0.2
0.3
0.4
1
2
3
W=3.00μm
D=3.35μm
VOPT
ESH
SH
(b)
B
V

Fig 5

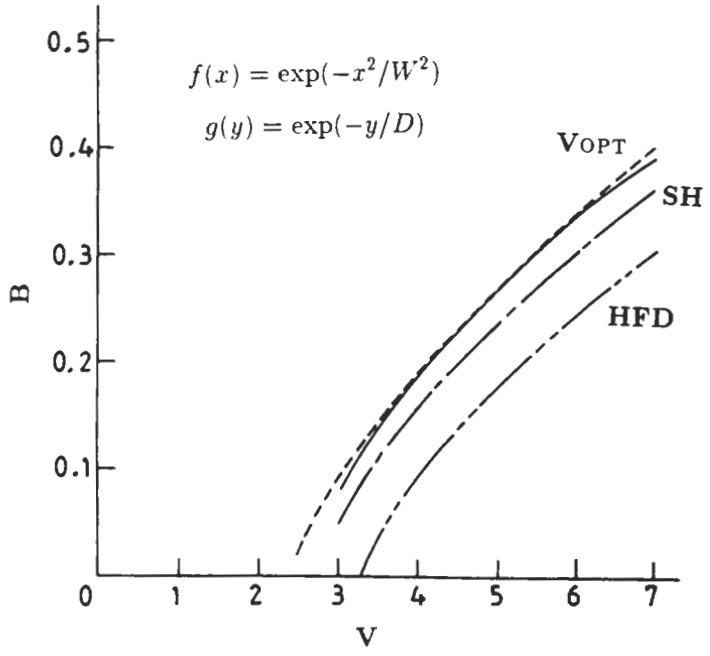

Fig 6

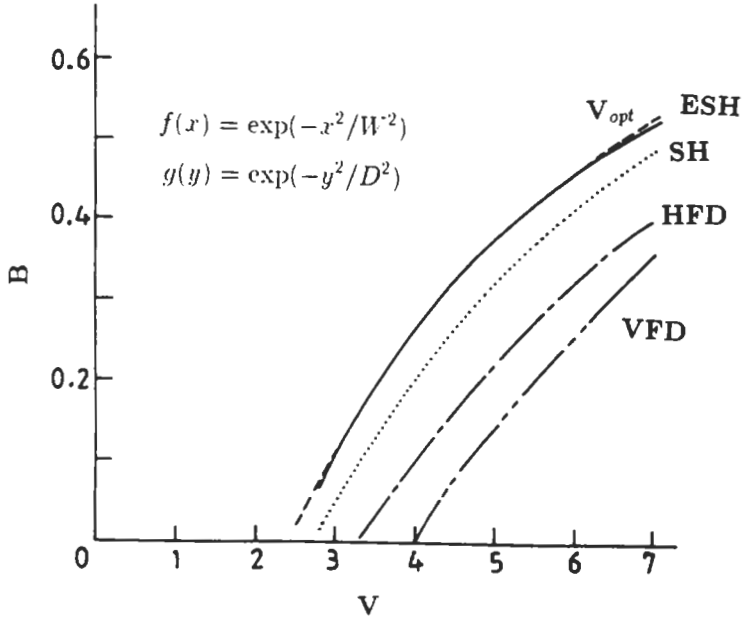

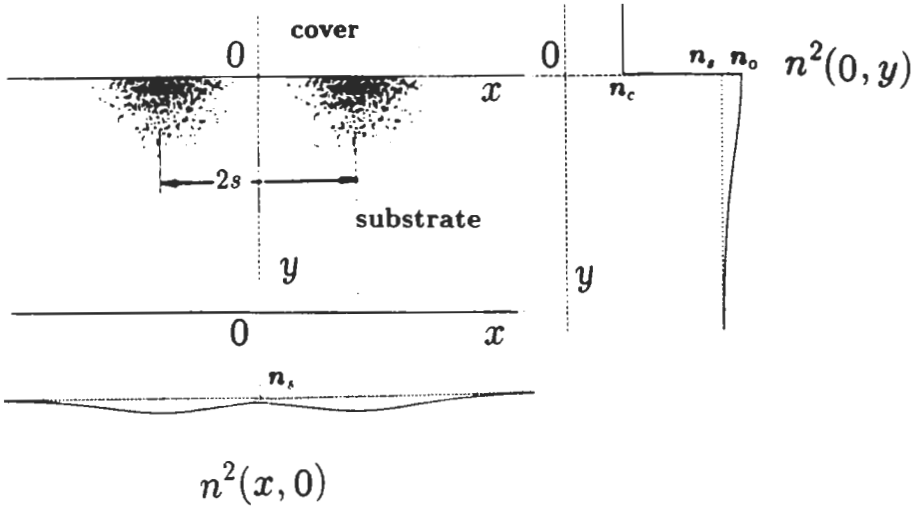

$n^2(x,0)$

Fig 8

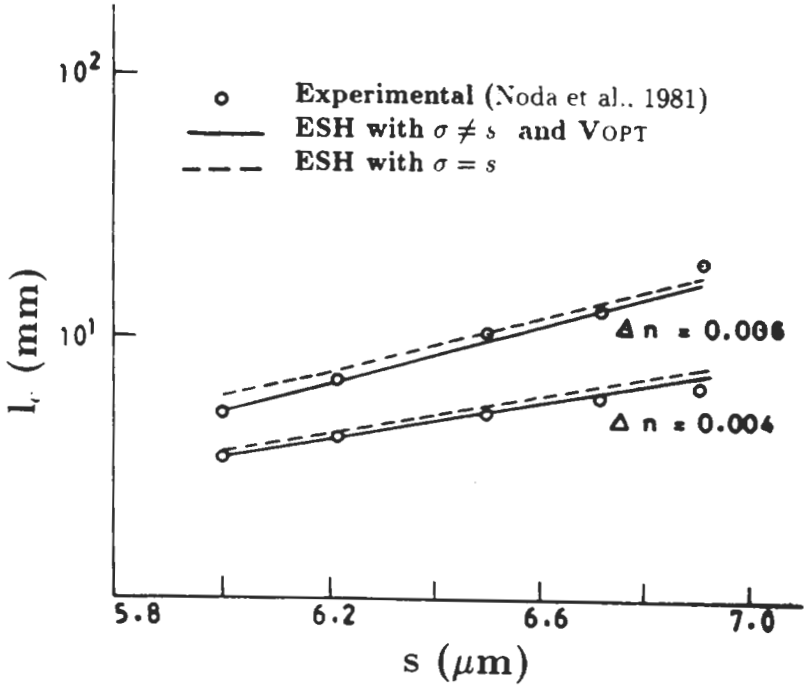
10^2
10^1
l_r (mm)
Experimental (Noda et al., 1981)
ESH with $\sigma \neq s$ and VOPT
ESH with $\sigma = s$
Δ n = 0.006
Δ n = 0.004
5.8
6.2
6.6
7.0
s (μm)

Fig 9

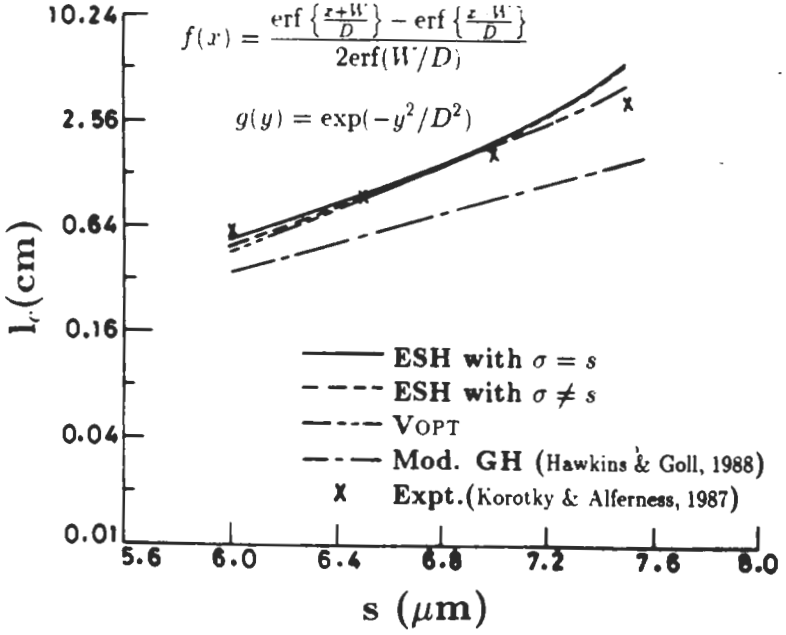
$f(x) = \frac{\mathrm{erf}\left\{\frac{x+W}{D}\right\} - \mathrm{erf}\left\{\frac{x-W}{D}\right\}}{2\mathrm{erf}(W/D)}$
$g(y) = \exp(-y^2/D^2)$
10.24
2.56
0.64
0.16
0.04
0.01
l_r(cm)
ESH with $\sigma = s$
ESH with $\sigma \neq s$
VOPT
Mod. GH (Hawkins & Goll, 1988)
Expt.(Korotky & Alferness, 1987)
5.6
6.0
6.4
6.8
7.2
7.6
8.0
s (μm)

Fig 10